

## SUPPLEMENTARY MATERIAL TO

### ‘Heat dissipation in partially-perforated phononic nano-membranes with periodicities below 100 nm’

A.M. Massoud<sup>a,b,†</sup>, V. Lacatena<sup>c,d,†</sup>, M. Haras<sup>c,d,†,£</sup>, E. Dubois<sup>c</sup>, S. Monfray<sup>d</sup>, J.-M. Bluet<sup>a</sup>, P.-O. Chapuis<sup>b</sup>, J.-F. Robillard<sup>c</sup>

<sup>a</sup> Univ Lyon, Institut des Nanotechnologies de Lyon (INL), CNRS, INSA de Lyon, F-69621 Villeurbanne, France.

<sup>b</sup> Univ Lyon, CNRS, INSA-Lyon, Université Claude Bernard Lyon 1, CETHIL UMR5008, F-69621, Villeurbanne, France.

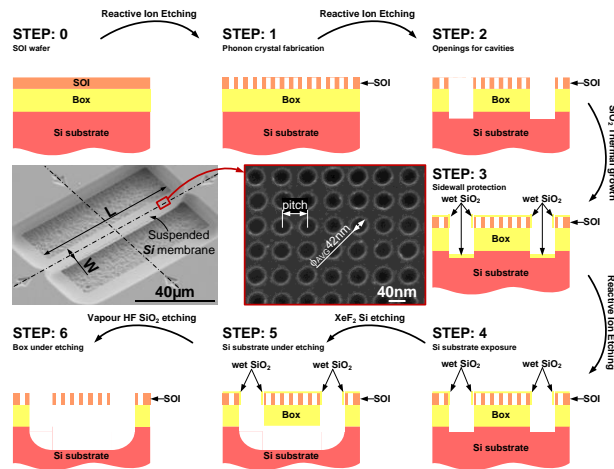
<sup>c</sup> Univ. Lille, CNRS, Centrale Lille, Junia, Univ. Polytechnique Hauts-de-France, UMR 8520 - IEMN – Institut d’Electronique de Microélectronique et de Nanotechnologie, F-59000 Lille, France.

<sup>d</sup> STMicroelectronics, 850, rue Jean Monnet, F-38926 Crolles, France.

In this document we provide supplementary information on various subjects related to the main paper.

#### Section 1: Fabrication process flow

The process flow is briefly detailed in the main paper. Suppl. Fig. 1 summarizes the main steps of the process.



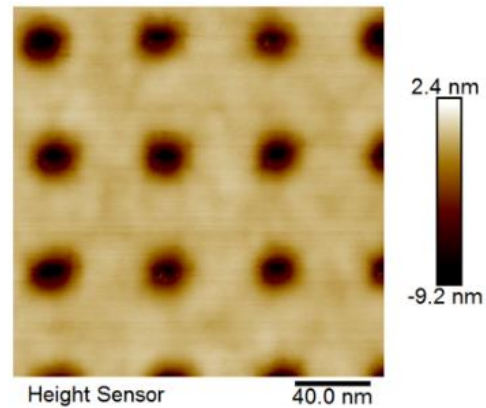
**Suppl. Fig. 1** Process flow used to fabricate the phononic thin-film silicon membranes

#### Section 2: Characterization of the phononic holes

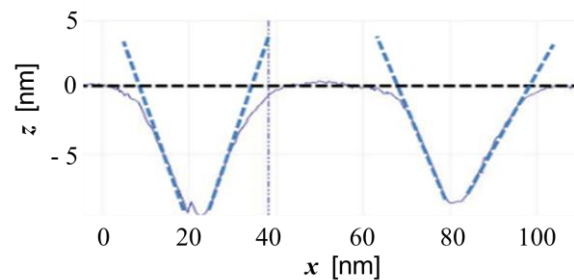
<sup>£</sup> Current address: CENTERA Laboratories, Institute of High Pressure Physics PAS, Sokołowska 29/37, 01-142 Warsaw, Poland; Centre for Advanced Materials and Technologies CEZAMAT, Warsaw University of Technology, Poleczki 19, 02-822 Warsaw, Poland

The geometrical dimensions of the membranes were investigated by means of scanning electron microscopy (SEM, see Fig. 1), scanning transmission electron microscopy (TEM, see also Fig. 1), and atomic force microscopy (AFM). The radii of the holes were determined both from SEM (including the white shells seen in the SEM top view of Fig. 1) and AFM.

(a)



(b)



**Suppl. Fig. 2.** Example of results from atomic force microscopy scans with sharp tip on the phononic crystals. (a) Full scan, (b) cross section. Dashed lines are guide to the eye.

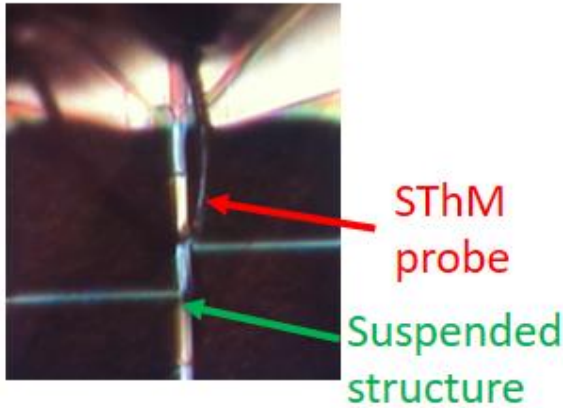
Final results of the geometrical studies are summarized in Suppl. Tab. 1. The uncertainty on the radius is close to 1 nm (found from the standard deviation in the SEM images over a large hole number), but there is some stronger uncertainty on the depth and exact shape of the holes. TEM cross section suggests that the holes could be spheriodal-like or paraboloids. Accounting for fabrication constrains, paraboloids are most likely. Note that the shape of the AFM cross section is difficult to analyze as the effect of convolution of the tip shape with the surface profile is not easy to eliminate in the tiny holes. However, such analysis provides a minimum depth for the holes.

The hole depth seems correlated with the radius, as small radii lead to smaller depths. The TEM depths are also minimal values as there is no guarantee that the cross sections were taken along the radii of the holes.

Pitch	SEM+AFM	Inner radius from SEM	Depth from AFM (avg)	Depth from TEM (noavg)
100 nm	21.5 nm	15.5 nm	21 nm	33 nm
80 nm	19 nm	13 nm	14 nm	x
60 nm	17.8 nm	11.4 nm	9 nm	16.5 nm

**Suppl. Tab. 1. Summary of the hole geometrical parameters. The depth of the 80 nm pitch was not investigated by TEM.**

### Section 3: Scanning membranes with STh



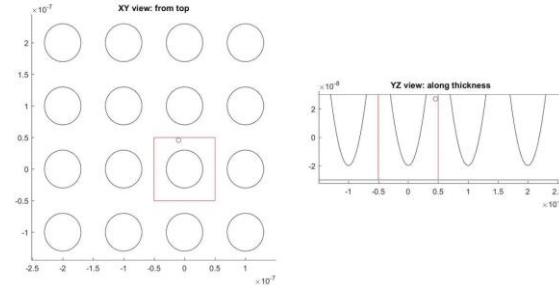
**Suppl. Fig. 3. View from top of a SThM Wollaston microprobe scanning the surface of a suspended membrane.**

Suppl. Fig. 3 provides an example of a SThM probe in contact with a suspended membrane. Here the membrane is a bit different from that of the core paper, as lateral

supporting arms are present. The membranes leading to the temperature profiles of Fig. 2 have the same shape as that shown in Fig. 1 of Ref. [1]. However this image provides an idea of the sizes involved in the experiment. Note also that the tip filament was parallel to the membrane in the experiment reported in the core paper, in contrast to the case of Suppl. Fig. 3 (see Ref.[1] for an example of filament aligned with the membrane).

### Section 4: Details on the Monte Carlo estimates of the mean free paths.

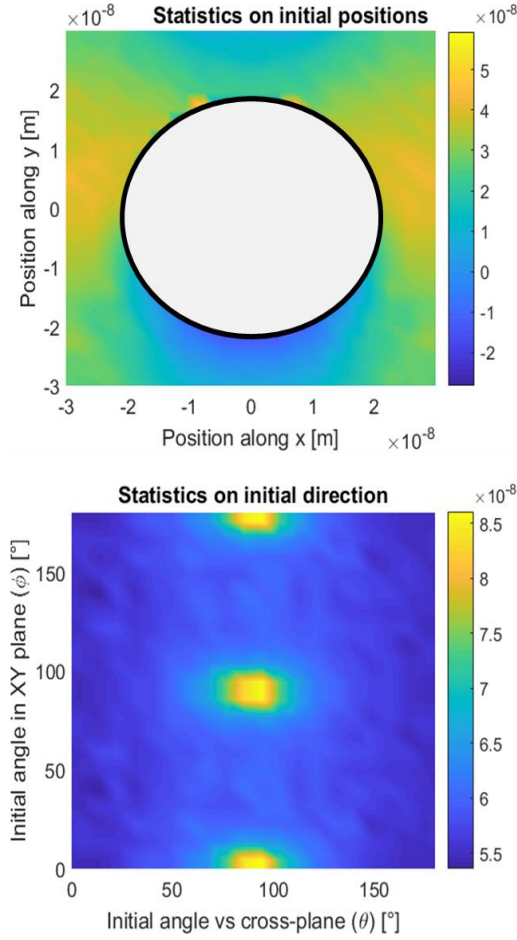
As shown in the Suppl. Video (see partial screenshot below), the trajectories of the phonons are followed in the phononic crystals. Both collisions with the membranes top/bottom sides and pores are treated diffusely in the main paper, in contrast to one of the videos. Phonon-phonon interactions are considered as extinctions of the phonon trajectories, so they do not appear in these videos.



**Suppl. Fig. 4. Partial screenshot of the Suppl. Video showing a phonon path projected onto the membrane plane (left) and on a cross section along the flux direction (right).**

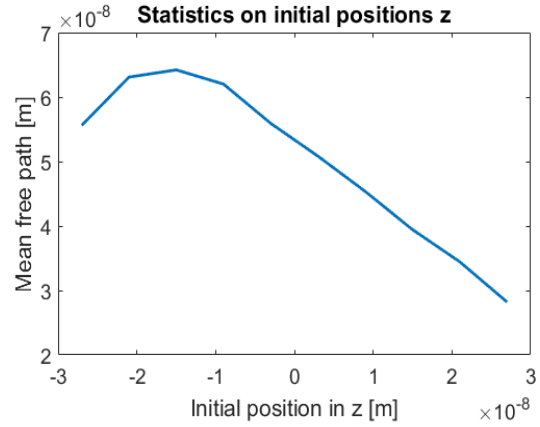
While the shapes of the holes change slightly for the different pitches (100 nm, 80 nm and 60 nm), the holes simulated were considered identical, with a radius  $R = 20$  nm and a depth  $h = 40$  nm in all the simulated data of the main paper.

In Suppl. Fig. 5, we provide the position and angle-dependent free path distributions for perforating cylindrical holes in a similar fashion as for Fig. 5 of the main paper. It is seen that free paths behind the holes become negative (Suppl. Fig. 5a), which is in agreement with the inset of Fig. 4 of the main paper, where it is seen that such holes strongly backscatter phonons. The effect is milder for the paraboloidal holes. Due to the large radii of the holes, only limited solid angle is available for the passage of the phonons, as shown in Suppl. Fig. 5b.



**Suppl. Fig. 5. Phonon free paths as a function of initial position and direction in the case of perforating cylindrical holes with mean free path 200 nm and  $R = 20$  nm (a) Average distance traveled in the flux direction as a function of initial angle. The circle underlines the position of the hole. (b) Average distance traveled as a function of initial position.**

Finally, we underline the  $z$ -dependent free path distribution in Suppl. Fig. 6, which shows results for the same membrane as that discussed in Fig. 5 of the main paper. It is seen that phonons can travel further in absence of hole, for negative  $z$  values. For a perforating membrane, the distribution would be symmetric.



**Suppl. Fig. 6. Phonon free paths as a function of initial position in the case of paraboloidal holes with mean free path 200 nm and ( $R = 20$  nm,  $h = 40$  nm).**

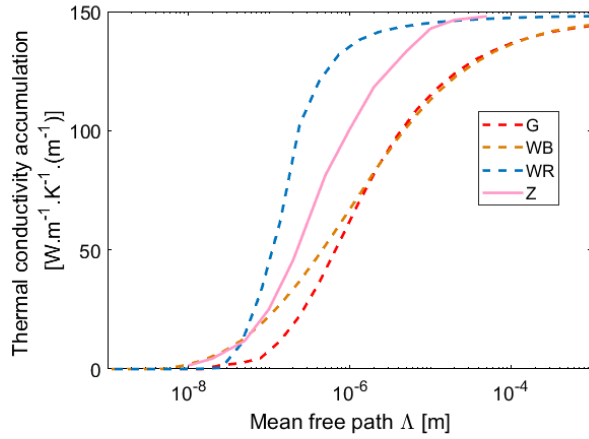
### **Section 5: Details on the mean free path distributions.**

The exact mean free path distribution of silicon is not known, so we tested various ones. Two strategies were applied:

(i) Relaxation times were obtained from different works, as for instance ab initio ones (WB) [2], molecular dynamics ones (G) [3], or analytical ones (used in Monte Carlo resolution of the Boltzmann Transport Equation, WR) [4]. They were used in conjunction with an isotropic dispersion of silicon taken by fitting the  $[1\ 0\ 0]$  direction with a parabolic expression that does not present maxima inside the Brillouin zone [5]. Since the product  $\int 1/3 c_p(\omega) v_g(\omega)^2 \tau(\omega) d\omega$  does not provide exactly  $148\text{ W}\cdot\text{m}^{-1}\cdot\text{K}^{-1}$  in this case (the atomic dispersion taken is not necessarily suitable for these relaxation times), the relaxation times were scaled homogeneously to provide the right thermal conductivity at 300 K.

(ii) The mean free path distribution determined from experimental investigations in [6] was directly used in Eq. (3) of the main paper (Z).

The distributions are compared in Suppl. Fig. 6. It is seen that some of them consider mean free paths larger than  $10\text{ }\mu\text{m}$  while other do not. This is therefore still a matter of debate.



**Suppl. Fig. 7. Accumulated bulk thermal conductivity of silicon as a function of mean free path, for various mean free path distributions. See text for legend. The abbreviations refer to the initials of the authors of the references cited in the main paper, except WR where the first initial refers to the first author of the reference [4] and the second to the first author of another reference mentioned in [4] where some of their data were obtained.**

While the distributions differ quite heavily we find in Fig. 6 of the main paper that their impacts on the effective thermal conductivities of the phononic crystal membranes are similar. The levels of thermal conductivities are however a bit different.

## Section 6: Effective medium approximations

There are various models that have been proposed for effective medium approximations (EMA), depending on the porosity, the randomness or not of the inclusions, and their shapes. Here we tested three models [7–9], which write as follows in the case of in-plane transport in membranes:

$$\begin{aligned} \text{Eucken:} \quad & \lambda = \lambda_{\text{host}}(1 - P)(1 + P/2) \\ \text{Maxwell-Garnett:} \quad & \lambda = \lambda_{\text{host}}(1 - P)(1 + P) \\ \text{Russel:} \quad & \lambda = \lambda_{\text{host}}(1 - P^{2/3})(1 + P - P^{2/3}), \end{aligned}$$

where  $P$  is the porosity.

Here we have taken the host thermal conductivity as reduced in comparison with the bulk, following the approach in [10] where the effective thermal conductivity in a nanomaterial is a Matthiessen rule involving the average mean free path and a factor close to the volume/surface ratio  $4V/S$ . It is noticeable that the thermal conductivity of the

pristine membrane is very close to the actual measurement (see Fig. 6 of the main paper).

## References

- [1] A. M. Massoud, J.-M. Bluet, V. Lacatena, M. Haras, J.-F. Robillard, and P.-O. Chapuis, “Native-oxide limited cross-plane thermal transport in suspended silicon membranes revealed by scanning thermal microscopy,” *Appl. Phys. Lett.*, vol. 111, no. 6, p. 63106, Aug. 2017.
- [2] A. Ward and D. A. Broido, “Intrinsic phonon relaxation times from first-principles studies of the thermal conductivities of Si and Ge,” *Phys. Rev. B*, vol. 81, no. 8, p. 85205, Feb. 2010.
- [3] J. V. Goicochea, M. Madrid, and C. Amon, “Thermal Properties for Bulk Silicon Based on the Determination of Relaxation Times Using Molecular Dynamics,” *J. Heat Transfer*, vol. 132, no. 1, Jan. 2010.
- [4] B. T. Wong, M. Francoeur, and M. Pinar Mengüç, “A Monte Carlo simulation for phonon transport within silicon structures at nanoscales with heat generation,” *Int. J. Heat Mass Transf.*, vol. 54, no. 9, pp. 1825–1838, 2011.
- [5] P. O. Chapuis, “Chapter 3: Introduction to heat transfer at the nanoscale,” in *Thermometry at the Nanoscale: Techniques and Selected Applications*, L. D. Carlos and F. Palacio, Eds. London: RSC Publishing, 2016.
- [6] L. Zeng *et al.*, “Measuring Phonon Mean Free Path Distributions by Probing Quasiballistic Phonon Transport in Grating Nanostructures,” *Sci. Rep.*, vol. 5, no. 1, p. 17131, 2015.
- [7] S. Alaie, D. F. Goettler, M. Su, Z. C. Leseman, C. M. Reinke, and I. El-Kady, “Thermal transport in phononic crystals and the observation of coherent phonon scattering at room temperature,” *Nat. Commun.*, vol. 6, no. 1, p. 7228, 2015.
- [8] D. Song and G. Chen, “Thermal conductivity of periodic microporous silicon films,” *Appl. Phys. Lett.*, vol. 84, no. 5, pp. 687–689, Jan. 2004.
- [9] L. Yang, N. Yang, and B. Li, “Extreme Low Thermal Conductivity in Nanoscale 3D Si Phononic Crystal with Spherical Pores,” *Nano Lett.*, vol. 14, no. 4, pp. 1734–1738, Apr. 2014.
- [10] A. Minnich and G. Chen, “Modified effective medium formulation for the thermal conductivity of nanocomposites,” *Appl. Phys. Lett.*, vol. 91, no. 7, p. 73105, Aug. 2007.